Glycobiology, 2023, **33**, 1, 75–85
https://doi.org/10.1093/glycob/cwac063
Advance access publication date 22 September 2022
Original Article

Anti-SARS-CoV-2 and anticoagulant properties of *Pentacta pygmaea* fucosylated chondroitin sulfate depend on high molecular weight structures

Rohini Dwivedi[1], Poonam Sharma[2], Friederike Eilts[3,4], Fuming Zhang[3], Robert J Linhardt[3], Ritesh Tandon[1,2,5], Vitor H Pomin[1,6,*]

[1]Department of BioMolecular Sciences, University of Mississippi, Oxford, Mississippi 38677, United States, [2]Center for Immunology and Microbial Research, Department of Cell Biology, University of Mississippi Medical Center, Jackson, MS 39216, United States, [3]Center for Biotechnology and Interdisciplinary Studies, Rensselaer Polytechnic Institute, Troy, NY 12180, United States, [4]Institute of Bioprocess Engineering and Pharmaceutical Technology, University of Applied Sciences Mittelhessen (THM), Giessen 35390, Germany, [5]Department of Medicine, University of Mississippi Medical Center, Jackson, MS 39216, United States, [6]School of Pharmacy, Research Institute of Pharmaceutical Sciences, University of Mississippi, Oxford, MS 38677, United States

*Corresponding author: Email: vpomin@olemiss.edu

Fucosylated chondroitin sulfate (FucCS) is a unique marine glycosaminoglycan that exhibits diverse biological functions, including antiviral and anticoagulant activity. In previous work, the FucCS derived from *Pentacta pygmaea* (PpFucCS) showed moderate anticoagulant effect but high inhibitory activity against the Wuhan strain of severe acute respiratory syndrome coronavirus (SARS-CoV-2). In this study, we perform free-radical depolymerization of PpFucCS by the copper-based Fenton method to generate low molecular weight (MW) oligosaccharides. PpFucCS oligosaccharides were structurally analyzed by ^{1}H nuclear magnetic resonance spectroscopy and were used to conduct structure–activity relationship studies regarding their effects against SARS-CoV-2 and clotting. Anticoagulant properties were measured by activated partial thromboplastin time, protease (factors Xa and IIa) inhibition by serine protease inhibitors (antithrombin [AT] and heparin cofactor II [HCII]), and competitive surface plasmon resonance (SPR) assay using AT, HCII, and IIa. Anti-SARS-CoV-2 properties were measured by the concentration-response inhibitory curves of HEK-293T-human angiotensin-converting enzyme-2 cells infected with a baculovirus pseudotyped SARS-CoV-2 Delta variant spike (S)-protein and competitive SPR assays using multiple S-proteins (Wuhan, N501Y [Alpha], K417T/E484K/N501Y [Gamma], L542R [Delta], and Omicron [BA.2 subvariant]). Cytotoxicity of native PpFucCS and oligosaccharides was also assessed. The PpFucCS-derived oligosaccharide fraction of the highest MW showed great anti-SARS-CoV-2 Delta activity and reduced anticoagulant properties. Results have indicated no cytotoxicity and MW dependency on both anti-SARS-CoV-2 and anticoagulant effects of PpFucCS, as both actions were reduced accordingly to the MW decrease of PpFucCS. Our results demonstrate that the high-MW structures of PpFucCS is a key structural element to achieve the maximal anti-SARS-CoV-2 and anticoagulant effects.

Key words: fucosylated chondroitin sulfate; nuclear magnetic resonance; oligosaccharide; SARS-CoV-2 inhibition.

Introduction

Severe acute respiratory syndrome coronavirus (SARS-CoV-2) is an enveloped betacoronavirus and causal pathogen of the COVID-19 pandemic (Hu et al. 2020). Glycosylated spike protein (S-protein) receptor-binding domain (RBD) present on the envelope of SARS-CoV-2 is the primary mode of contact with the host-cell heparan sulfate proteoglycans (HSPGs) and angiotensin-converting enzyme-2 (ACE2) receptor during the infectivity (Clausen et al. 2020). This interaction is key to membrane fusion, internalization of the virus particle in the host cell, and subsequent infection (Belouzard et al. 2012).

Multiple random mutations in the SARS-CoV-2 (Wuhan-Hu-1 strain) genome has led to a series of rapidly emerging viral variants (Cosar et al. 2022). Some of these variants have highly mutated S-protein, which is directly responsible for the increased pathogenicity of the strain (Harvey et al. 2021). The World Health Organization has classified the SARS-CoV-2 variants of concern (VOC) based on multiple features such as transmissibility, virulence, transmission, capability of evading diagnosis and therapeutic interventions, and general disease symptoms (Thakur et al. 2022). Among all currently circulating VOCs, Delta (B.1.617.2) and Omicron (B.1.1.529) are those with highest transmissibility and virulence. Delta variant (B.1.617.2), which was first identified in India, has been recognized as the most aggressive variant so far (Thakur et al. 2022). The high pathogenicity of Delta variant is adjudged to the 10 amino acid mutations in its S-protein of which 3 are considered as key mutations (L452R, T478K, and P681R) (Aleem et al. 2022). This has resulted in significant immune evasion and high transmissibility of this VOC, consequently leading to additional wave of the pandemic (Planas et al. 2021; Saito et al. 2021; Tian et al. 2021).

Development of potential medicines capable of treating the pathological consequences of COVID-19 and inhibiting the infectivity of a broad range of emerging variants is increasingly important. Different classes of molecules are being investigated as the probable anti-SARS-CoV-2 inhibitors (Shyr et al. 2020; Xiu et al. 2020). Some of these rely on the inhibitory strategy of disrupting the viral S-protein binding with the host cell surface HSPG and ACE2. The competitive inhibition of S-protein-HSPG binding by sulfated glycans, like heparin and heparin mimetics (sulfated polysaccharides and synthetic heparin mimetics), has shown to effectively inhibit SARS-CoV-2 (Wuhan-Hu-1 strain) infection in multiple pseudovirus- and live virus-based assays (Tandon et al. 2021; Guimond et al. 2022). However, sulfated glycans can be also potent anticoagulant agents (Pereira et al. 1999; Farias et al. 2000; Wu et al. 2015; Mourão 2015). Hence, discovery of

Received: July 14, 2022. **Revised:** September 12, 2022. **Accepted:** September 12, 2022

naturally potent anti-SARS-CoV-2 sulfated glycans with reduced anticoagulant properties or the dissociation of the anticoagulant and anti-SARS-CoV-2 properties are 2 possible ways to overcome these anticoagulant side effects. In previous works, we were able to give examples of these 2 cases (Dwivedi et al. 2021; Kim et al. 2022). A new fucosylated chondroitin sulfate (FucCS) from the body wall of the sea cucumber *Pentacta pygmaea* (PpFucCS) showed moderate anticoagulant but high anti-SARS-CoV-2 activity against the Wuhan-Hu-1 strain as compared to the gold standard heparin (Dwivedi et al. 2021). In another study, molecular weight (MW) reduction of the highly anticoagulant sulfated galactan from the red alga *Botryocladia occidentalis* (BoSG) was capable to select the anti-SARS-CoV-2 property by significant depletion of its anticoagulant effect (Kim et al. 2022).

In this work, we examine the effects of MW on the functions of PpFucCS as anticoagulant and anti-SARS-CoV-2 molecule. For this, we performed free-radical depolymerization of PpFucCS to selectively cleave the backbone of this sulfated glycan to produce oligosaccharides for further use in biological studies. 1D ^{1}H nuclear magnetic resonance (NMR) spectroscopy is used to assess structural information of PpFucCS oligosaccharides. Anticoagulant properties of PpFucCS oligosaccharides were assessed by activated partial thromboplastin time (aPTT) and inhibitory effects of coagulation proteases, factors IIa (thrombin), and Xa by serine protease inhibitors (serpins), antithrombin (AT), and heparin cofactor II (HCII). Investigation of the SARS-CoV-2 activity of native PpFucCS and its oligosaccharides is extended to the more infectious SARS-CoV-2 Delta strain using HEK-293T expressing human ACE2 (HEK-293T-hACE2) cells using a baculovirus pseudotyped with SARS-CoV-2 S-protein (Delta strain) and to multiple strains (Wuhan, N501Y [Alpha], K417T/E484K/N501Y [Gamma], L542R [Delta], and Omicron [BA.2 subvariant]) by competitive surface plasmon resonance (SPR). Current results have indicated that the native high-MW structure of PpFucCS is required for its inhibitory effects against coagulation and SARS-CoV-2 infection.

Results and discussion

Extraction and purification of PpFucCS

Extraction of PpFucCS was achieved by papainolytic digestion of the dried body wall of sea cucumber *P. pygmaea* as reported earlier (Dwivedi et al. 2021). Digested crude extract upon anion exchange chromatographic purification yielded pure PpFucCS when eluted using a linear gradient of NaCl (0–3 M) (Supplementary Fig. S1). Purity and structural integrity of native PpFucCS preparation were confirmed by 1D ^{1}H NMR spectrum (Supplementary Fig. S2, top spectrum). The 1D ^{1}H NMR spectrum of purified PpFucCS showed absence of any solvent impurities or contaminants and presence of only characteristic ^{1}H NMR signals of the PpFucCS structure (Fig. 1A). These ^{1}H NMR signals are indicated as A, B, C, and D in the α-anomeric region (δ_H 5.9–5.3 ppm) for the following 4 fucose (Fuc) branching units, α-Fuc2,4S, α-Fuc2,4S, α-Fuc4S, and α-Fuc0S; the β-anomeric region (δ_H 5.2–4.5 ppm) of the *N*-acetylgalactosamine (GalNAc) and glucuronic acid (GlcA) of the FucCS backbone, ring ^{1}H signal region (δ_H 5.0–3.5 ppm), and the far upfield methyl region of GalNAc and Fuc (δ_H 2.4–1.2 ppm) (Dwivedi et al. 2021).

Free-radical depolymerization of PpFucCS

Branching mono- or di-Fuc units and sulfation patterns are the functional structural feature of the PpFucCS structure {→3)-β-GalNAcX-(1 → 4)-β-GlcA-[(3 → 1)Y]- (1→}, where X = 4S (80%), 6S (10%), or nonsulfated (10%); Y = α-Fuc2,4S (40%), α-Fuc2,4S-(1 → 4)-α-Fuc (30%), or α-Fuc4S (30%) (Fig. 1A). Free-radical depolymerization by modified Fenton chemistry has been proven to be efficient in producing structurally intact FucCS oligosaccharides (Li et al. 2017) through selective cleavage of the glycosidic bonds between the backbone GlcA and GalNAc residues (Li et al. 2016). We performed depolymerization of PpFucCS using copper-based Fenton chemistry under the conditions described previously to prevent extensive defucosylation or desulfation in the FucCS structure (Li et al. 2016). The H_2O_2 concentration (source of free radical), copper concentration, temperature, pH, and time are key factors that contribute to the quality of the Fenton reaction. Hence, we examined different concentrations of H_2O_2 (20 mM, 100 mM, and 200 mM) and $Cu(OAc)_2$ (0.02 mM, 0.2 mM, and 2 mM) for the successful and controlled depolymerization of PpFucCS at 60 °C and pH 6.0. Supplementary Figure S3 shows 2 of these tested conditions. Among all examined conditions, PpFucCS (2 mg in 0.1 M NaOAc, pH 6.0) treated with 200 mM H_2O_2 in the presence 0.02 mM $Cu(OAc)_2$ at 60 °C was selected. Progress of the reaction was monitored at different time durations, 15 min, 30 min, 60 min, 180 min, and 360 min. The reaction mixture was quenched using chelex resin (50–100 mesh size) at different time points to choose the optimal reaction duration.

The MW distribution and the structural integrity of the PpFucCS oligosaccharides produced were investigated by polyacrylamide gel electrophoresis (PAGE; Fig. 1B) and 1D ^{1}H NMR spectroscopy (Fig. 1C). The 1D ^{1}H NMR analyses of the reaction mixtures at 3 intermittent time points (30 min, 60 min, and 180 min) indicated the intactness of the repeating unit of the molecule (Fig. 1C). The characteristic 1D ^{1}H NMR peaks of the α-anomeric protons in the branching Fuc (α-Fuc2,4S (A), α-Fuc2,4S (B), α-Fuc4S (C) and α-Fuc0S (D)) at the above time points were found resonating in the same original region (δ_H 5.9–5.3 ppm) (Fig. 1C) with constant relative peak integral values. The methyl peaks of GalNAc and Fuc resonate in the original region of δ_H at 2.4–1.4 ppm like those in the native PpFucCS spectrum (Fig. 1C and Supplementary Table S1). The constant integral ratio of GalNAc-COC$\underline{H}_3$ and Fuc-C$\underline{H}_3$ methyl peaks upon depolymerization confirms no defucosylation and, thus, a selective cleavage solely at the backbone glycosidic linkages. The similar chemical shifts of the α-anomeric ^{1}H peaks of branching Fuc in the depolymerized products as compared to the native PpFucCS rule out any potential desulfation occurring at the Fuc units upon depolymerization process. Production of shorter chain oligosaccharides than the native PpFucCS was monitored as a function of depolymerization time (Fig. 1B). Among all time courses tested, 180 min was optimal for formation of oligosaccharides in a similar range of the low-MW heparin (LMWH) for further fractionation in size exclusion chromatography (SEC). Hence, approximately, 40 mg of pure PpFucCS was then depolymerized under these conditions for the scaled-up production of oligosaccharides to SEC fractionation and structure–activity relationship studies.

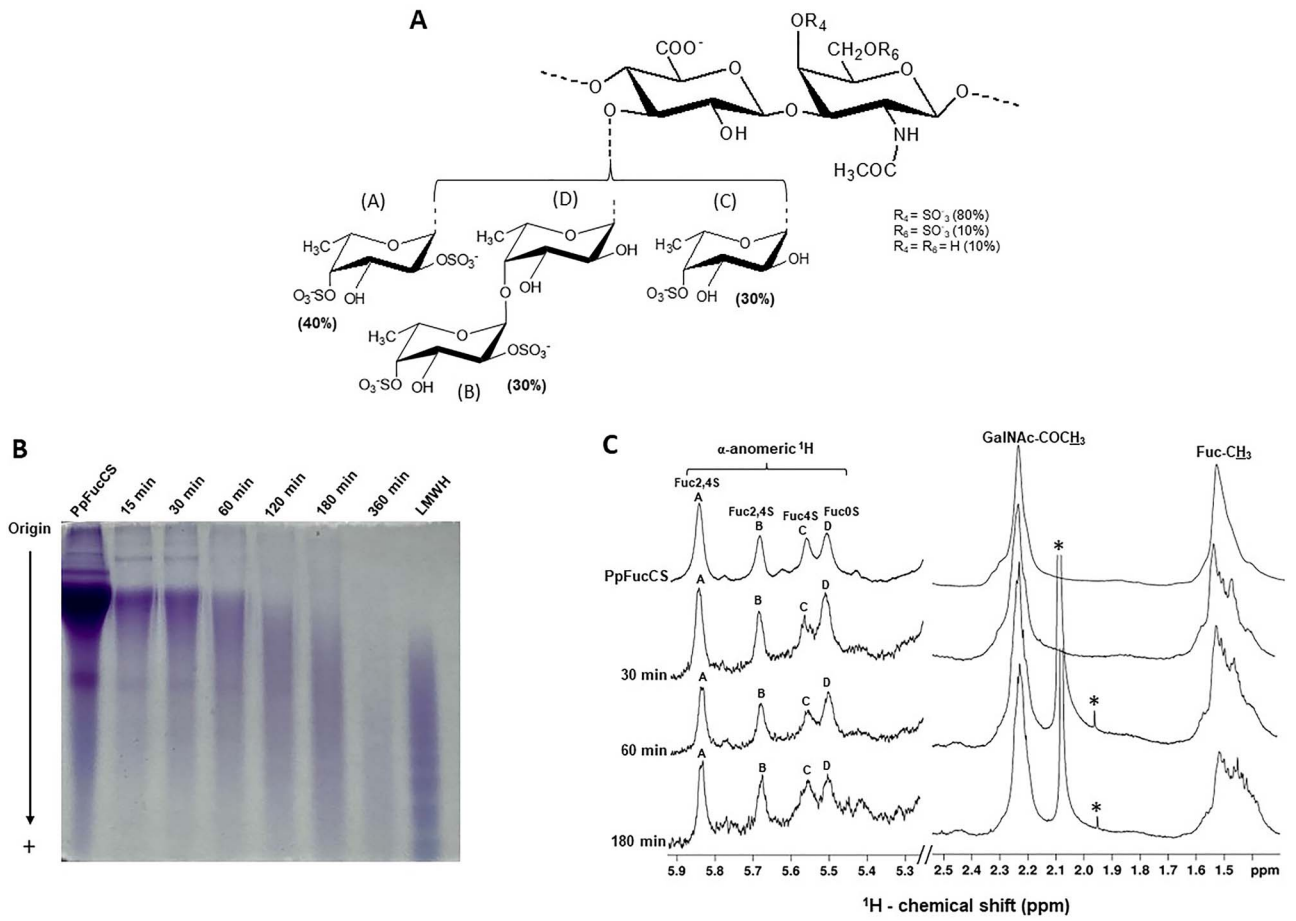

Fig. 1. Free-radical depolymerization of PpFucCS by copper-based fenton method. A) Structural representation of PpFucCS, showing a chondroitin sulfate backbone of alternating GalNAc and GlcA in repeating disaccharide units of [→3)-β-GalNAc-(1 → 4)-β-GlcA-(1→]$_n$, where the GalNAc units are mostly 4-sulfated (80%), 6-sulfated (10%), or nonsulfated (10%). The GlcA units are substituted at the C3 position by 3 types of α-Fuc branches: 40% [Fuc2,4S-(1→] (A unit in NMR), 30% [Fuc2,4S-(1 → 4)-Fuc-(1→] (B → D units in NMR), and 30% [Fuc4S-(1→] (C unit in NMR), where S = SO_3^-. B) Optimization of free-radical depolymerization reaction conditions of PpFucCS achieved by copper-based Fenton method—2 mg/mL of PpFucCS depolymerized by 0.02 mM copper (II) acetate and 200 mM H_2O_2 for different durations: 15 min, 30 min, 60 min, 120 min, 180 min, and 360 min. MW distribution of the depolymerized reaction mixture was analyzed by PAGE using the molecular markers: LMWH, and native PpFucCS. C) 1D ^{1}H NMR spectra were recorded in D_2O, at 50 °C, on a 500 MHz Bruker NMR instrument for the native PpFucCS and its depolymerized reaction mixture at 3 time points (30 min, 60 min, and 180 min). The NMR signals corresponding to characteristic fucosyl branches in the α-anomeric region (δ_H expansion 5.9–5.3 ppm) of the depolymerized products obtained at different time points are labeled on top of the spectral stack as A (Fuc2,4S), B (Fuc2,4S), C (Fuc4S), and D (Fuc0S). Upfield region (δ_H expansion 2.5–1.4 ppm) diagnostic of ^{1}H signals from the protons of GalNAc-COC$\underline{H}_3$ and of Fuc-C$\underline{H}_3$ shows the characteristic methyl peaks from native PpFucCS and oligosaccharide mixtures. The signals indicated with asterisks are from solvent.

Fractionation of depolymerized PpFucCS oligosaccharides

The mixture of PpFucCS oligosaccharides from hydrolyzed PpFucCS (HdPpFucCS) obtained after a 180-min Fenton reaction was then fractionated by SEC using a Bio-Gel P-10 column. Oligosaccharides were eluted with 10% ethanol in 1 M NaCl and assayed for metachromicity with 1,9-dimethymethylene blue (DMB). The chromatogram in Fig. 2A shows the elution profile of PpFucCS oligosaccharides. The lack of narrow peaks in the chromatogram indicates the continuous dispersion of oligosaccharide distribution in the HdPpFucCS as previously noticed by the polydisperse nature seen in PAGE (Figs. 1B and 2B) unlike the distinct narrow bands seen for LMWH in PAGE which translate into well-defined peaks on the Bio-Gel P10 chromatogram (Supplementary Fig. S4; Oliveira et al. 2015). The undefined SEC profile of HdPpFucCS was still able to produce low-MW fraction of PpFucCS, which were labeled as Fr1–Fr4 based on their respective elution time. Oligosaccharide fractions were assayed for their respective MW distribution by PAGE (Fig. 2B). The MW distribution was assessed in comparison with mammalian glycosaminoglycans of known MWs: LMWH, unfractionated heparin (UFH), and chondroitin sulfate-C (CS-C).

Structural analysis of PpFucCS oligosaccharides

Fractionated PpFucCS oligosaccharides were subjected to 1D ^{1}H NMR spectral analysis to investigate their structures. The decrease in the size of the PpFucCS chain length did not compromise the structural integrity of the repeating unit in most of the produced oligosaccharides (Fig. 2C). The ^{1}H chemical shift values (Table 1) of the α-anomeric signals of Fuc units in PpFucCS, HdPpFucCS, and Fr1–3 show clear evidence of the presence of the 4 units as in the native PpFucCS structure—α-Fuc2,4S (δ_H 5.83 ppm), α-Fuc2,4S (δ_H 5.76 ppm), α-Fuc4S (δ_H 5.64 ppm), and α-Fuc0S (δ_H 5.59 ppm; Fig. 2C). This

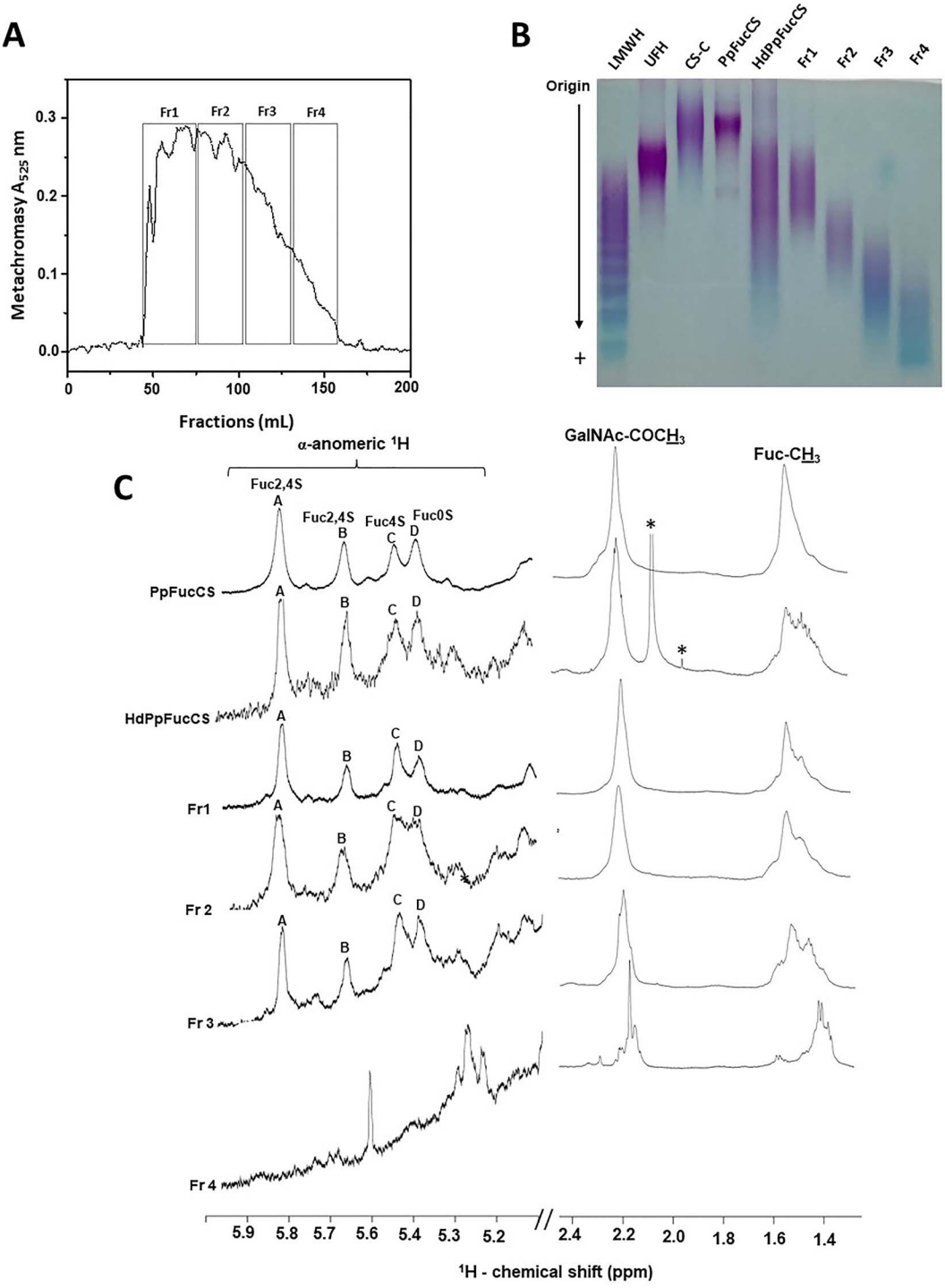

Fig. 2. Fractionation and structural characterization of PpFucCS oligosaccharides. A) Depolymerized PpFucCS (40 mg) obtained through free-radical depolymerization using 0.02 mM copper acetate, 200 mM H_2O_2 for 180 min, was fractionated on a Bio-Gel P10 column (1.5 cm × 170 cm) using 10% ethanol in 1 M NaCl as elution buffer. Multiple fractions (1 mL each) were collected at a flow rate of 1.0 mL/15 min. Fractions were individually analyzed by metachromatic assay using 1,9-dimethylmethylene blue (Abs 525 nm) for the presence of oligosaccharides. The fractions corresponding to the respective peaks, were pooled, and labeled as Fr1–Fr4. B) MW distribution of native PpFucCS, unfractionated depolymerized PpFucCS (HdPpFucCS), and the purified PpFucCS oligosaccharides (Fr1–Fr4) were analyzed by PAGE using a series of molecular markers: LMWH, UFH, and CS-C. C) 1D ^{1}H NMR spectral stack showing the expansion from the α-anomeric region (δ_H expansion 5.9–5.3 ppm) and the methyl region (δ_H expansion 2.5–1.4 ppm) of the fractionated oligosaccharides (Fr1–Fr4), HdPpFuccS, and native PpFucCS. 1D ^{1}H NMR spectra confirmed the presence of the 2 mono-Fuc branches (α-Fuc2,4S and α-Fuc4S) and 1 di-Fuc branch (α-Fuc2,4S-(1 → 4)-α-Fuc), attached to the C3 position of the GlcA linked to GalNAc unit in the backbone of all fractions, except Fr4. Fraction 4 exhibits an upfield ^{1}H shift of the Fuc anomeric peaks, suggesting possible desulfation. Peaks are labeled as A, B, C, and D corresponding to 4 α-Fuc units: Fuc2,4S, Fuc2,4S, Fuc4S, and Fuc0S. All 1D ^{1}H NMR spectra were acquired at 50 °C on a 500 MHz Bruker NMR instrument. The signals indicated with asterisks are from solvent.

Table 1. ^{1}H chemical shift (δ_H, ppm) values of α-anomerics (^{1}H1) of branching Fucs (A-D), acetyl methyl groups of GalNAc, and fucosyl methyl groups from PpFucCS and oligosaccharides

	δ_H (ppm)[a]				
Unit	PpFucCS	HdPpFucCS	Fr1	Fr2	Fr3
Fuc2,4S (A)	5.83	5.84	5.85	5.86	5.84
Fuc2,4S (B)	5.76	5.68	5.69	5.70	5.68
Fuc4S (C)	5.64	5.56	5.57	5.57	5.55
Fuc0S (D)	5.59	5.50	5.52	5.52	5.50
GalNAc-C$\underline{H}_3$	2.30	2.22	2.20	2.24	2.23
Fuc-C$\underline{H}_3$	1.50	1.51	1.52	1.52	1.52

[a] Chemical shift values were acquired at 500 MHz at 50 °C and referenced to external trimethylsilylpropionic acid for 0 ppm for ^{1}H.

confirms that Fr1–Fr3 have same structures but different sizes. The broadening of the Fuc methyl peak (δ_H 1.5 ppm) could be attributed to the changes associated with cleavage of bonds in the backbone affecting the chemical shift profile of the Fuc-C$\underline{H}_3$ groups in the formed oligosaccharides (Fig. 2C). The ^{1}H-^{13}C heteronuclear single quantum coherence (HSQC) spectrum of the depolymerized PpFucCS mixture at 180 min (HdPpFucCS) confirmed the integrity of the sulfation pattern in the GalNAc units since the NMR signal profile looks like the HSQC spectrum of the native molecule (Supplementary Fig. S5 and Supplementary Table S2).

Fr 4 with the smallest size distribution in PAGE (Fig. 2B), however, exhibited a different NMR spectral profile as compared to the native PpFucCS and other fractions (Fig. 2C). A significant different pattern of ^{1}H NMR peaks in the α-anomeric region of the Fr4 indicates multiple chemical changes accompanying the drastic MW reduction, likely due to extensive desulfation as the ^{1}H signals move toward the upfield region. Nonetheless, the Fenton chemistry was demonstrated to preserve the structural integrity of the native PpFucCS in most of the oligosaccharides produced (Fr1–Fr3), and just a small percentage of the very low-MW (Fr4) appeared more chemically modified. The blue staining of Fr4 as opposed to the purple coloration of Fr1–Fr3 in PAGE (Fig. 2B) and the very low metachromatic property at Bio-Gel P-10 chromatogram (Fig. 2A) support the low sulfation content observed by 1D ^{1}H NMR (Fig. 2C). Regardless of desulfation in Fr4, together with Fr1–Fr3, all fractionated PpFucCS oligosaccharides showed the same original peak integral ratio of GalNAc-C$\underline{H}_3$ and FucC$\underline{H}_3$, demonstrating no defucosylation by the Fenton reaction. Full 1D ^{1}H NMR spectra of all PpFucCS fractions are displayed in Supplementary Fig. S6.

Anticoagulant activities of PpFucCS oligosaccharides

The MW reduction has been shown to impact anticoagulant activity of FucCS, in general (Li et al. 2017). We examined the anticoagulant properties of the 4 PpFucCS fractions (Fr1–Fr4), HdPpFucCS, native PpFucCS, and UFH by aPTT assay and serpin-mediated inhibitory assays to investigate the structure-activity relationship of PpFucCS. Results indicate a significant decrease in prolonging the coagulation time of all fractions compared to native PpFucCS (Fig. 3A). HdPpFucCS and Fr1 show an aPTT value of 6 IU/mg and 12 IU/mg in comparison to 30 IU/mg exhibited by native PpFucCS (Table 2). The Fr2, Fr3, and Fr4 demonstrated a significant compromised aPTT prolongation (Fig. 3A, Table 2). We performed AT-dependent IIa and Xa inhibition and HCII-dependent IIa inhibition to further investigate the effects of oligosaccharides and MW reduction in the activity of the serpin-mediated protease inhibition (Fig. 3B–D). The aPTT and IC_{50} values of the oligosaccharides are presented in Table 2. The serpin-mediated analysis demonstrates a significant loss in both AT and HCII inhibition of IIa and Xa as all PpFucCS low-MW products did not exhibit the half-maximum inhibitory concentration at the highest tested concentration (100 μg/mL). This result indicates a size-dependent phenomenon to the anticoagulant property of PpFucCS. The Fr1 (IC_{50} = 4.7 μg/mL) and HdPpFucCS (IC_{50} = 9.6 μg/mL; Fig. 3B), however, exhibited a residual HCII-IIa activity compared to the lower MW oligosaccharides Fr2, Fr3, and Fr4 in Fig. 3B. This residual action was not observed in the case of AT-mediated inhibition of IIa and Xa by the oligosaccharides (Fig. 3C and D), which is the more predominant system in the coagulation cascade, explaining therefore the very low activity seen by the general aPTT assay (Fig. 3A).

Anti-SARS-CoV-2 activity and cytotoxicity of PpFucCS oligosaccharides

PpFucCS is a potent anti-SARS-CoV-2 molecule which exhibits its inhibitory activity by its competitive inhibition of SARS-CoV-2 S-protein binding to host-cell HSPGs (Dwivedi et al. 2021). Here, we investigate the inhibitory activity of both PpFucCS and low-MW products against Delta variant (a more virulent and infectious strain compared to the previously studied Wuhan strain) using the technology of green fluorescent protein (GFP) transduction in HEK-293T-hACE2 cells infected with pseudotyped SARS-CoV-2 S-protein (Delta variant). The low-MW PpFucCS products studied here were used to correlate the effect of MW distribution on its anti-SARS-CoV-2 action against the Delta strain. The SPR-based results discussed further will give insights regarding the MW contribution in the anti-SARS-CoV-2 action of PpFucCS in other strains.

From the inhibitory concentration-response curves, it was interesting to see that the native PpFuccS exhibits potent and efficacious inhibitory action against SARS-CoV-2 Delta variant comparable to UFH, while oligosaccharides show a decrease in activity (Fig. 4A and Table 2). Comparison of the low-MW PpFucCS products show that HdPpFucCS and Fr1 can retain higher efficacy than Fr2, Fr3, and Fr4, while showing marginally less than native PpFucCS and UFH (see I_{max} values in Table 2). Results clearly demonstrate a decrease in the activity of PpFucCS oligosaccharides in a size-dependent manner as we analyze the activities from Fr1 to Fr4. Fr4, with the lowest MW distribution, appears to significantly lose its antiviral activity as it starts a plateau very below the

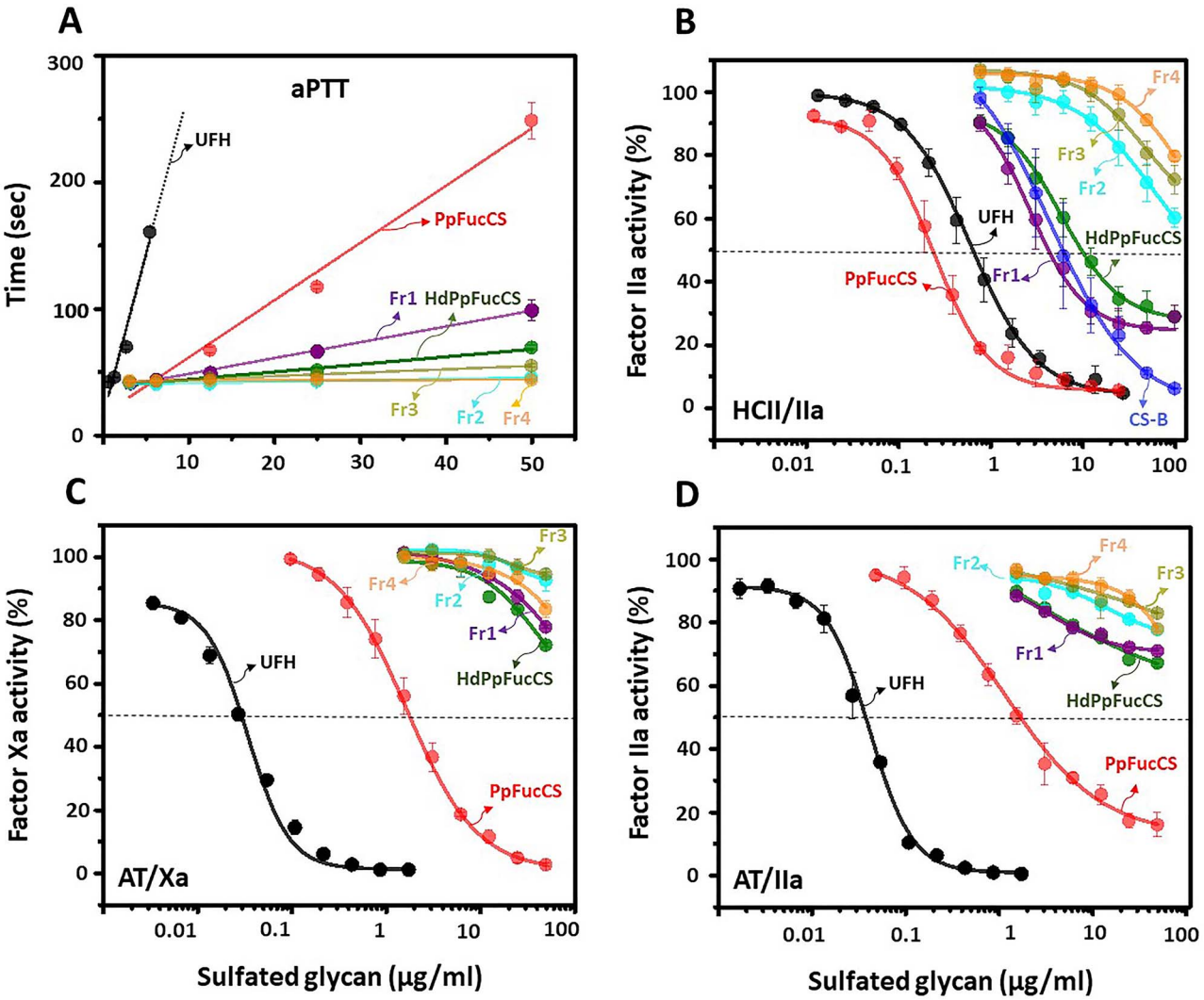

Fig. 3. Anticoagulant concentration-response of PpFucCS oligosaccharides. A) aPTT, B) HCII-mediated factor IIa inhibition, C) AT-mediated factor Xa inhibition, and D) AT-mediated factor IIa inhibition. The polysaccharides examined (in a concentration range up to 50 μg/mL) for the anticoagulant activity included UFH, CS-B, PpFucCS, HdPpFucCS, Fr1, Fr2, Fr3, and Fr4. The dotted line in panels B-D indicate the half-maximal inhibitory activity of the polysaccharides. The concentrations of coagulation (co)factors used in the experiments were 10 nM of AT or HCII and 2 nM of factors IIa or Xa. Each experiment was performed in triplicates and each point in plotted data represents the mean ± SD of the triplicated set.

Table 2. IC_{50} values of anticoagulant and anti-SARS-CoV-2 Delta (B.1.617.2) activities of UFH, PpFucCS, and PpFucCS oligosaccharides

Glycan	Anticoagulant activity				Anti-SARS-CoV-2 (B.1.617.2)[a]	
	aPTT (IU/mg)[b]	HCII/IIa IC_{50} (μg/mL)	AT/Xa	AT/IIa	IC_{50} (μg/mL)	I_{max}
UFH	180	0.6 ± 0.07	0.025 ± 0.06	0.03 ± 0.003	0.3 ± 0.2	98.4 ± 0.8
PpFucCS	30.2 ± 0.02	0.2 ± 0.02	1.8 ± 0.2	1.2 ± 0.07	0.5 ± 0.3	98 ± 0.2
HdPpFucCS	6.6 ± 0.44	9.6 ± 1.3	ND[c]	ND	5.4 ± 1.4	94.7 ± 2.7
Fr1	12 ± 0.19	4.7 ± 0.8	ND	ND	3 ± 0.2	96.5 ± 1.0
Fr2	ND	ND	ND	ND	0.2 ± 0.2	75.8 ± 4.5
Fr3	ND	ND	ND	ND	0.3 ± 0.5	56 ± 8.6
Fr4	ND	ND	ND	ND	ND	28 ± 15.5
CS-B	-	6.2 ± 2.1	-	-	-	-

[a]IC_{50} values of anti-SARS-CoV-2 inhibitory activity of UFH, PpFucCS, and PpFucCS oligosaccharides were determined against HEK 293T-hACE2 cells infected with baculovirus pseudotyped with SARS-CoV-2 S-protein of the Delta variant. Each value is mean ± SD of triplicate measurements. [b]Values were calculated using a parallel UFH (180 IU/mg) standard curve. Each value is mean ± SD of triplicate measurements. [c]ND, not determined.

half-maximum inhibitory concentration level with a very low concentration (Fig. 4A). The IC_{50} values, derived from the anti-SARS-CoV-2 Delta variant analysis, are shown in Table 2. PpFucCS and its oligosaccharides do not exhibit cytotoxicity against HEK 293T cells when examined at the highest concentration used in the antiviral assay (50 mg/L; Fig. 4B)

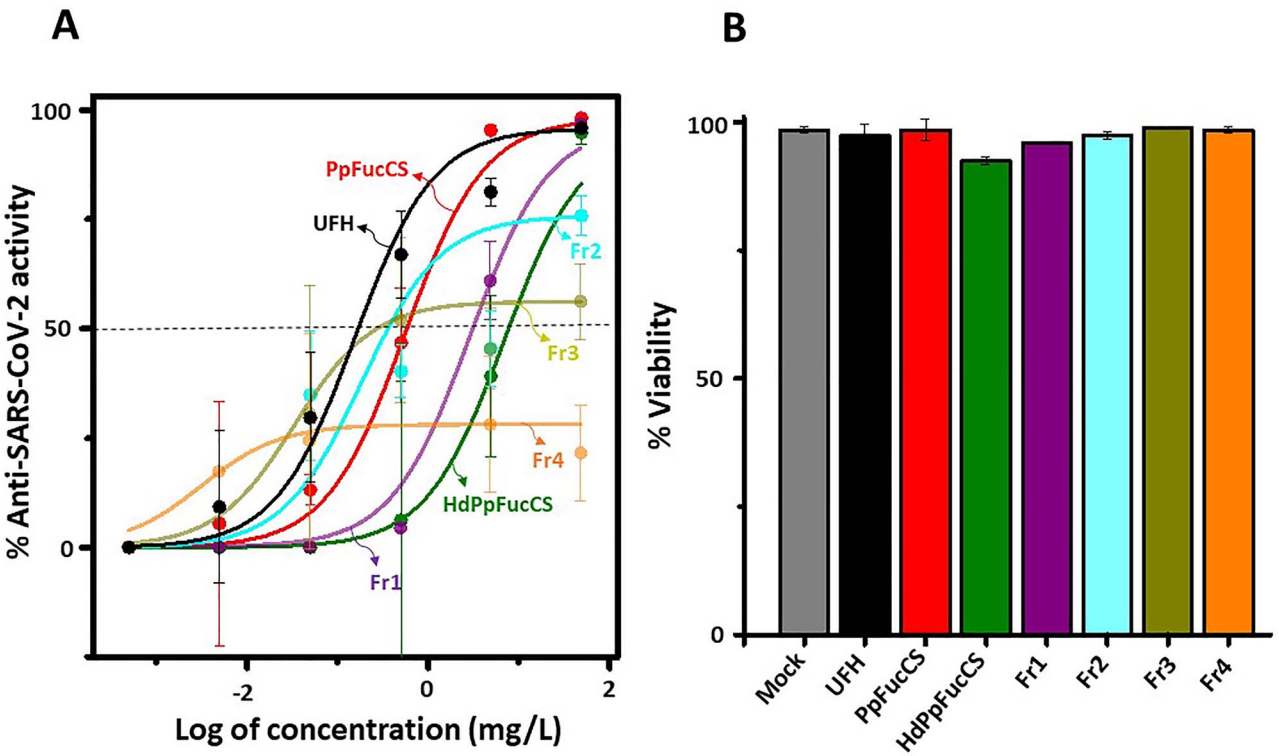

Fig. 4. Anti-SARS-CoV-2 Delta (B.1.617.2) and cytotoxic activities of PpFucCS oligosaccharides. A) PpFucCS oligosaccharides were assayed for their potential to inhibit GFP transduction in HEK-293T-hACE2 cells infected with pseudotyped SARS-Cov-2 S-protein Delta variant. Normalized values from the assay were analyzed by nonlinear regression to fit a dose–response curve using the least squares method considering each replicate value as an individual point. The plotted curve shows percentage of SARS-CoV-2 Delta variant inhibition in a (log) concentration-dependent manner. Curves in the plot represent the following: UFH, PpFucCS, HdPpFucCS, Fr1, Fr2, Fr3, and Fr4. B) Bar plots represent percentage cell viability of HEK-293T-hACE2 cells when treated with the above-mentioned sulfated glycans at the highest examined concentration (50 mg/L). Each experiment was performed in triplicates and each point in plotted data represents the mean ± SD of the triplicate set.

and at a concentration of 500 mg/L to disregard any toxic potential close to the studied range (Supplementary Fig. S7). Interestingly, among all tested fractions, the PpFucCS-derived oligosaccharide fraction of the highest MW, Fr1, showed great activity against the Delta variant as compared to the native PpFucCS and UFH and reduced anticoagulant effect.

Binding of PpFucCS and oligosaccharides to SARS-CoV-2 S-protein RBDs and blood (co)-factors

The interactions between the coagulation (co)-factors and S-protein RBDs of different SARS-CoV-2 variants with native PpFucCS, PpFucCS oligosaccharides, and UFH was investigated by SPR to explain the observed decrease actions of PpFucCS in anticoagulation and anti-SARS-CoV-2 (multiple VOCs) and to compare the activities of PpFucCS and derivatives with UFH. The binding of the 8 tested proteins to the 7 sulfated glycans was examined through the competitive inhibition SPR assay using heparin immobilized on the streptavidin (SA)-coated sensor chip. Figure 5 illustrates the plots presenting normalized protein bindings of glycans: AT (Fig. 5A), HCII (Fig. 5B), IIa (Fig. 5C), SARS-CoV-2 WT RBD (Fig. 5D), SARS-CoV-2 N501Y (Alpha) RBD (Fig. 5E), SARS-CoV-2 L542R (Delta) RBD (Fig. 5F), SARS-CoV-2 triple mutant K417T/E484K/N501Y (Gamma) RBD (Fig. 5G), and SARS-CoV-2 Omicron (BA.2 subvariant) RBD (Fig. 5H). Values in Table 3 depict the percent inhibition in binding of the respective proteins to the surface heparin caused by the 7 sulfated glycans.

SPR-based results with the coagulation proteins indicate that PpFucCS and low-MW derivatives have lower affinity for AT than UFH (Fig. 5A), which correlates well with the observed lower activity in AT/Xa and AT/IIa inhibitory systems of Fig. 3C and D. Results also reveal that the direct binding of PpFucCS oligosaccharides to IIa to be only marginally less than UFH (Fig. 5C). As expected, the PpFucCS and its low-MW oligosaccharides generally exhibit strong binding to HCII (Fig. 5B), explaining the observed strong action of PpFucCS and residual action of oligosaccharides (HdPpFucCS and Fr1) when tested in the HCII/IIa system (Fig. 3B).

Regarding the different RBDs, the PpFucCS oligosaccharides show a clear decrease in binding in a size-dependent manner (Fig. 5D–H). Among all oligosaccharide fractions tested, Fr1 exhibited comparatively higher binding in all the examined RBDs. The SPR-based results have demonstrated that the native high-MW PpFucCS structure is efficient to bind to all tested RBDs and with stronger affinity than UFH (Table 3). Inhibition was slightly less effective against the Omicron RBD (BA.2 subvariant) RBD but still higher than UFH for most of the PpFucCS derivatives (Fig. 5H). The contribution of MW in the inhibitory interaction of PpFucCS and derivatives with Delta RBD corroborates the MW-dependent mechanism observed in the cell-based experiment of Fig. 4. Native PpFucCS presents significant binding inhibition of RBDs from 2 circulating VOCs, Delta (100%), and Omicron (85%). In all, the SPR-based analyses (Fig. 5) have clearly supported our previous findings that

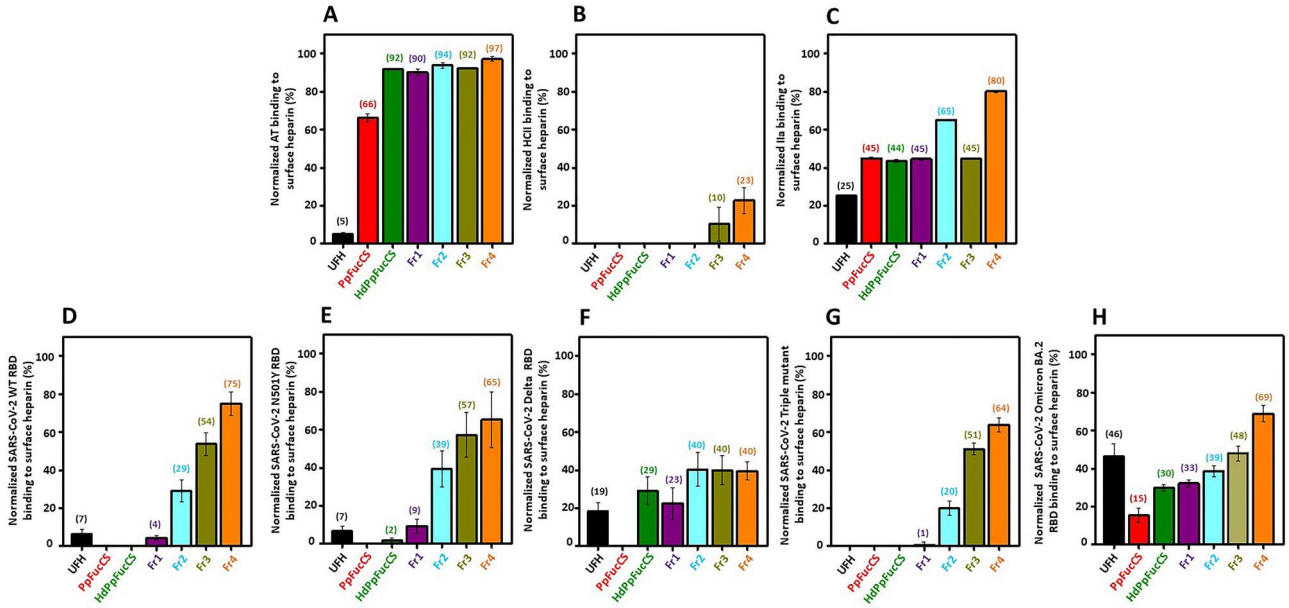

Fig. 5. Competitive SPR binding of blood (co)-factors and SARS-CoV-2 RBDs to surface heparin in the presence of sulfated glycans. The bar plots indicate normalized binding of A) AT, B) HCII, C) thrombin (IIa), and SARS-CoV-2 RBDs of D) WT, E) Alpha N501Y mutant, F) Delta L542R mutant, G) Gamma triple K417T/E484K/N501Y mutant, and H) Omicron (BA.2 subvariant) to surface heparin-immobilized sensorchip in the presence of UFH, PpFuCS and fragments. UFH, PpFucCS, HdPpFucCS, Fr1, Fr2, Fr3, and Fr4. The numbers on top of each bar indicate the average normalized binding value obtained in the experiments. The normalization has been measured with respect to only protein bound to the surface heparin. Each experiment was performed in triplicates and each point in plotted data represents the mean ± SD of the triplicate set.

Table 3. Inhibitory percentage of exogenous sulfated glycans in competitive SPR binding of coagulation Serpins (AT and HCII), factor IIa, and SARS-CoV-2 S-protein RBDs (WT and variants) to heparin-immobilized sensor chip

Glycan	Blood (co)-factors			SARS-CoV-2 S-protein RBDs				
	AT	HCII	IIa	WT	N501Y	Delta	Triple mutant	Omicron BA.2
UFH	95 ± 0.7	100	75 ± 0.3	93 ± 2.5	93 ± 2.6	81 ± 4.5	100	54 ± 6.7
PpFucCS	34 ± 2.2	100	55 ± 0.4	100	100	100	100	85 ± 3.8
HdPpFucCS	8 ± 0.3	100	56 ± 0.8	100	98 ± 1.5	71 ± 7.2	100	70 ± 1.7
Fr1	10 ± 1.6	100	55 ± 0.6	96 ± 1.2	91 ± 3.7	77 ± 8.1	99 ± 1.6	67 ± 1.9
Fr2	6 ± 1.4	100	35 ± 0.5	71 ± 5.6	61 ± 9.5	60 ± 8.7	80 ± 3.7	61 ± 2.9
Fr3	8 ± 0.5	90 ± 8.9	55 ± 0.6	46 ± 5.9	43 ± 11.9	60 ± 7.6	49 ± 3.2	52 ± 3.8
Fr4	3 ± 1.2	77 ± 6.8	20 ± 0.7	25 ± 6.3	35 ± 14.6	60 ± 4.6	36 ± 3.7	31 ± 4.3

Values in the table were calculated by subtracting the normalized binding values (in %) from the control value (100%) which are just proteins alone. Normalized binding values were determined from competitive SPR measurements of the binding S-proteins and coagulation factors (serpins and protease) to surface heparin in the presence of UFH, PpFucCS, and PpFucCS oligosaccharides. Each value is mean ± SD of triplicate measurements.

the anticoagulant (Fig. 3) and anti-SARS-CoV-2 (Fig. 4) properties of PpFucCS are MW-dependent.

Conclusions

Free-radical depolymerization of PpFucCS by copper-based Fenton method was successfully employed in generating oligosaccharides with shorter chain lengths and conserved structural integrity like native PpFucCS. Our results suggest that native high MW of PpFucCS is a key structural element to achieve the maximal anticovid and anticoagulant effects. We can, however, consider the PpFucCS-derived oligosaccharide fraction Fr1 of highest MW as an interesting preparation for future studies, given its reduced anticoagulant property but still high anti-SARS-CoV-2 activity. As opposed to BoSG (linear sulfated galactan) whose anticoagulant and anti-SARS-CoV-2 actions are, respectively, dependent and independent of MW (Kim et al. 2022), these 2 biomedical activities are mostly dependent of high-MW in the case of PpFucCS (branched GAG). This indicates that the biomedical effects of marine sulfated poly/oligosaccharides can be dictated not only by only 1 structural feature but by a conjunction of structural features such as the combination of the native structure (linear homopolysaccharides versus branched GAG) and MW distribution.

Materials and methods

Extraction and purification of PpFucCS

PpFucCS was isolated from the body wall of the sea cucumber *P. pygmaea* (Gulf Specimen Lab Gulf of Mexico, Florida Keys) by proteolytic digestion using papain (Sigma, St. Louis, MO, United States), as reported earlier (Dwivedi et al. 2021). The dry crude extract was fractionated by anion exchange chromatography on a column (1.5 cm × 20 cm) packed with DEAE-Sephacel resin (Sigma). Elution was performed using a linear gradient of NaCl (in 0.1 M NaOAc, pH 6.0) from 0 M to 3 M at a flow rate of 0.5 mL/min. All the fractions were

monitored by 1,9-dimethylmethylene blue (DMB) reagent. The polysaccharide fractions positive for DMB assay were pooled and dialyzed 3 times against water and lyophilized. The dialyzed sugars were subsequently subjected to Sephadex G15 (Sigma) column (1 cm × 30 cm) purification using water as mobile phase for further cleanup. The purified sugar was dried by lyophilization. Dry weight was measured and used for the concentration estimation of the samples in the various assays.

Depolymerization of PpFucCS

PpFucCS was depolymerized employing the modified Fenton chemistry, which has been shown to be very selective for the cleavage of GlcA and GalNAc bonds present in the backbone of this class of polysaccharide. The reaction was performed following slightly modified version of an earlier reported protocol (Li et al. 2016). For the optimization of the reaction condition, 2 mg of dry PpFucCS was weighed and dissolved at a concentration of 2 mg/mL in 0.1 M sodium acetate, and pH 6.0. 0.02 mM copper (II) acetate (final concentration) was added to the dissolved polysaccharide solution. H_2O_2 at a final concentration of 200 mM was then added dropwise to the reaction mixture under continuous stirring and the reaction was carried out at 60 °C. Aliquots of reaction mixture were taken out at different time points: 15 min, 30 min, 60 min, 120 min, 180 min, and 360 min. Reaction at each time point was quenched by removing the copper ions from the reaction mixture using Chelex (50–100 mesh size) resin (Sigma). For quenching, Chelex resin preequilibrated with 0.1 M sodium acetate buffer, pH 6.0, was added to reaction mixture and kept on an end-to-end rotor for 2 h at room temperature. After 2 h, the suspension was centrifuged at 3,000 rpm for 10 min. Supernatant was lyophilized and desalted prior to further analysis. Under the standardized condition, the final reaction was performed for a duration of 180 min at 60 °C using 40 mg (dried weight) of PpFucCS dissolved at a concentration of 2 mg/mL in 0.1 M sodium acetate, with pH 6.0, having 0.02 mM copper (II) acetate and 200 mM H_2O_2.

Fractionation of depolymerized PpFucCS oligosaccharides

The dried depolymerized mixture of PpFucCS was fractionated based on size in a Bio-Gel P-10 column (1.5 cm × 170 cm; Bio-Rad Laboratories, Hercules, CA, United States). Fractionation of the mixture was carried out using 10% ethanol containing 1.0 M NaCl at a flow rate of 1.0 mL/15 min (Kim et al. 2022). Obtained fractions were assayed by DMB for the presence of PpFucCS oligosaccharides. Based on the DMB profile of eluted oligosaccharides, they were grouped into 4 fractions (Fr1–Fr4) according to their respective retention time on the Bio-Gel P-10 column. All the fractions were desalted on the Sephadex G-15 column followed by lyophilization prior to any analysis.

PpFucCS oligosaccharide distribution

The oligosaccharide distribution of the depolymerized PpFucCS fractions was assessed by running native PAGE along with MW standards: LMWH (~8 kDa), UFH (~15 kDa), CS-C (~60 kDa), and native sulfated glycan PpFucCS. Dried sugar samples were weighed and dissolved in water to form a concentrated solution of 2 mg/mL. Sample amount of 10 μg (in 50% glycerol, 0.5 M Tris, pH 6.8) was loaded on a 1.5-mm thick discontinuous PAGE system having 4% stacking gel and a 28% resolving gel phase. Electrophoretic migration was achieved under the conditions reported earlier.

Determination of structural integrity of PpFucCS oligosaccharides by NMR

The NMR sample of PpFucCS and depolymerized fractions were prepared by dissolving 1.5–2 mg (dry weight) of the respective polysaccharides in 200 μL D_2O (99.90%) (Cambridge Isotope Laboratories, Inc. Andover, MA, United States) in 3-mm NMR tubes (VWR International, Radnor, PA, United States). 1D ^{1}H NMR spectrum with a total of 512 number of scans were used for the complete acquisition. The ^{1}H-^{13}C HSQC spectra of PpFucCS and HdPpFucCS (Supplementary Fig. S5) were acquired using, respectively, T_1 and T_2 acquisition times of 0.121 s and 0.005 s and 1,024 × 256 points and 1,024 × 128 points. Acquisition was done via double INEPT transfer using Echo/Antiecho TPPI gradient selection with decoupling during acquisition and trim pulses during the INEPT transfer. All ^{1}H NMR and ^{1}H-^{13}C HSQC spectra of HdPpFucCS were acquired on a 500-MHz Bruker magnet, while the ^{1}H-^{13}C HSQC spectrum of PpFucCS was acquired on a 600-MHz Bruker NMR. Acquired NMR data were further processed and analyzed using TopSpin 4.0 software.

Determination of AT/HCII dependent inhibition of IIa/Xa by PpFucCS oligosaccharides

PpFucCS oligosaccharides were assayed for their serpin-mediated inhibitory activity against IIa and Xa at an effective concentration of 10 nM of AT or HCII, 2 nM of IIa or factor Xa, and 0–100 μg/mL of sulfated glycans in 100 μL of TS/PEG buffer (0.02 M Tris/HCl, 0.15 M NaCl, and 1.0 mg/mL polyethylene glycol 8000, pH 7.4) as reported earlier (Vasconcelos et al. 2018). Oligosaccharides (10 μL) at serial diluted concentrations were dispensed in the 96-well microtiter plate, followed by the addition of 40 μL AT (25 nM) or HCII (25 nM). The reaction was initiated by adding 50 μL of IIa (4 nM) or Xa (4 nM). The plate was then immediately incubated at 37 °C for 1 min, which was followed by the addition of 25 μL of chromogenic substrate S-2238 (Chromogenix, AB, Mondal, Sweden) for IIa or CS-11(32) (Aniara Diagnostica, West Chester, OH, United States) for factor Xa. The absorbance (Abs) was then measured at 405 nm for 300 s at an interval of 15 s. Wells without oligosaccharides served as control and was considered to be 100% for IIa/Xa activity. The residual IIa/Xa activity in oligosaccharide-treated wells was calculated relative to that observed in the case of control wells. Heparin (183 IU/mg) and PpFucCS were used in all the assays as a positive control. DS (CS-B) was also used as a positive control in the HCII/IIa system. All the aPTT assay reagents were procured from Thermo Fisher Scientific (Waltham, MA, United States), and the coagulation factors Xa, IIa, AT, and HCII were from Haematologic Technologies. Sigma. All the assays were performed 3 times. Calculated IC_{50} values represent mean ± standard deviation (SD) obtained from the triplicated measurements. Supplementary Table S3 shows the statistical values.

Viral inhibition of PpFucCS oligosaccharides

The virus inhibitor screening was done on human embryonic kidney cells (HEK-293T) expressing human ACE2 (HEK-293T-hACE2 cell line, BEI Resources #NR-52511) plated in a 96-well tissue culture plate using a baculovirus pseudotyped with SARS-CoV-2 Delta-variant spike protein containing a green fluorescent reporter (Montana Molecular, #C1123G; Dwivedi et al. 2021; Tandon et al. 2021; Yan et al. 2021). Virus titers were confirmed by enumerating GFP-positive transduced cells in a dilution under a fluorescence microscope (EVOS-FL, Thermo Fisher Scientific) and multiplying by the dilution factor and the volume plated. Serial dilutions (50 mg/L, 5 mg/L, 0.5 mg/L, 0.05 mg/L, 0.005 mg/L, 0.0005 mg/L, and 0.00005 mg/L) of the test PpFucCS oligosaccharides were made in DMEM in triplicates to the final volume of 100 μL in each well. The controls used were UFH at 50 mg/L and mock-treated cells. Then, 2.5 μL of the pseudotype virus stock (2×10^{10} units per mL) was mixed with the test compounds and incubated for 1 h, which was then laid over HEK-293T-hACE2 cells plated in a 96-well plate along with 2 mM of sodium butyrate. Plate was then incubated for 60 h and the assay was read on a Cytation 5 automated fluorescence microscope after fixing with 3.7% formaldehyde. The relative IC_{50} values were calculated in Prism 9 (Graphpad Inc) by plotting the normalized values from the assay against the concentrations (log) of oligosaccharides and controls and analyzing by nonlinear regression to fit a dose–response curve using the least squares method considering each replicate value as an individual point. Each experiment was performed in triplicate. Supplementary Table S4 shows the statistical values.

Cytotoxicity of PpFucCS oligosaccharides

Cytotoxic activity of oligosaccharides was determined against the HEK-293T-hACE2 cells seeded in 12-well tissue culture plates following the protocol reported earlier (Dwivedi et al. 2021; Tandon et al. 2021). The confluent HEK-293T-hACE2 cells were treated with oligosaccharides at a final concentration of 50 mg/L and 500 mg/L along with 2 mM sodium butyrate. The treated cells were harvested after 60 h of incubation and examined via trypan blue exclusion assay for viability. Assay readout was measured on a TC20 automated cell counter (BioRad) according to the manufacturer's protocol. Assay was performed in triplicate and the values are plotted as mean ± SD of % live cells.

Competitive SPR reagents

SARS-CoV-2 S-Protein RBD (WT) and mutants (N501Y [Alpha], triple mutant [K417T/E484K/N501Y; Gamma], and L542 mutant [Delta]) were provided by Prof. Bates, University of Mississippi. Omicron RBD (BA.2 subvariant) was purchased from Sino Biological US Inc (Wayne, PA, USA). Human AT, HCII, and α-thrombin (IIa) were from Haematologic Technologies (Essex Junction, VT). Sensor SA chips were from Cytiva (Uppsala, Sweden). SPR measurements were performed on a BIAcore 3000 operated using 3000 control and Biaevaluation software version 4.0.1. (Uppsala, Sweden).

Preparation of heparin for SPR

Heparin (2 mg) and amine-PEG3-Biotin (2 mg, Pierce, Rockford, IL) were dissolved in 200 μL H_2O, and 10 mg $NaCNBH_3$ was added. The reaction mixture was heated at 70 °C for another 24 h and after that a further 10 mg $NaCNBH_3$ was added and the reaction was heated at 70 °C for another 24 h. After cooling to room temperature, the mixture was desalted with the spin column (3000 MWCO). Biotinylated heparin was collected, freeze-dried, and used for SA chip preparation. The biotinylated heparin was immobilized to SA chip based on the manufacturer's protocol. In brief, 20 μL solution of biotinylated heparin (0.1 mg/mL) in HBS-EP running buffer was injected over flow cell 2 (FC2) of the SA chip at a flow rate of 10 μL/min. The successful immobilization of heparin was confirmed by the observation of a ~200 resonance unit (RU) increase in the sensor chip. The control flow cell (FC1) was prepared by 1-min injection with saturated biotin.

Competitive solution SPR study of sulfated glycans

Solution competition study between the surface heparin and soluble different sulfated glycans was performed using SPR. In brief, protein samples mixed with sulfated glycans (100 μg/mL) in HBS-EP buffer were injected over heparin chip at a flow rate of 30 μL/min, respectively. After each run, the chip was regenerated with 2 M NaCl injection. For each set of competition experiments on SPR, a control experiment (with only protein) was performed. Normalized binding of the proteins to surface heparin in the presence of sulfated glycans was determined with respect to control values. This was calculated by dividing the obtained RU values of each experiment (using various glycans) by the control values. Each experiment was repeated in triplicate and the results were presented as the mean ± SD of the 3 experiments.

Supplementary data

Supplementary material is available at *Glycobiology* Journal online.

Funding

This work was supported by NIH (grant numbers 1P20GM 130460-01A1-7936 and 1R03NS110996-01A1) and the University of Mississippi grant to V.H.P. NASA award (#80NSSC19K1603) and NIH award (1R01DE031928-01A1) supported the work in the laboratory of R.T. This work was supported by the NIH (AG069039-01 and DK111958) and GlycoMIP, a National Science Foundation Materials Innovation Platform funded through Cooperative Agreement (DMR-1933525 to R.J.L. and F.Z.).

Conflict of interest statement: No conflict of interest to disclose.

Data availability

The authors declare that the data supporting the findings of this study are available within the article and its supplementary information file.

Authors' contributions

V.H.P. did the conceptualization; R.D, P.S., F.Z., R.T., and V.H.P. performed the methodology; R.D., P.S., F.Z., R.T., and V.H.P. did the validation; R.D., P.S., F.E., F.Z., and

V.H.P. carried out the formal analysis; R.D., P.S., F.E., and F.Z. performed the investigation; F.Z., R.J.L., R.T., and V.H.P. were responsible for the resources; R.D., P.S., F.E., and F.Z. carried out data curation; R.D., F.Z., and V.H.P. performed writing—original draft; R.D., R.J.L., R.T, and V.H.P. performed writing–review & editing; R.D., F.Z., R.T., and V.H.P. were in charge of the visualization; F.Z., R.T., and V.H.P. were responsible for the supervision; V.H.P. carried out project administration; F.Z., R.J.L., R.T., and V.H.P. took care of funding acquisition. All authors agreed with the manuscript.

References

Aleem A, Akbar Samad AB, Slenker AK. Emerging variants of SARS-CoV-2 and novel therapeutics against coronavirus (COVID-19)-PubMed. In: *StatPearls*. Tampa, Florida, United States: StatPearls Publishing; 2022.

Belouzard S, Millet JK, Licitra BN, Whittaker GR. Mechanisms of coronavirus cell entry mediated by the viral spike protein. *Viruses*. 2012:**4**(6):1011–1033.

Clausen TM, Sandoval DR, Spliid CB, Pihl J, Perrett HR, Painter CD, Narayanan A, Majowicz SA, Kwong EM, McVicar RN et al. SARS-CoV-2 infection depends on cellular heparan sulfate and ACE2. *Cell*. 2020:**183**(4):1043–1057.e15.

Cosar B, Karagulleoglu ZY, Unal S, Ince AT, Uncuoglu DB, Tuncer G, Kilinc BR, Ozkan YE, Ozkoc HC, Demir IN et al. SARS-CoV-2 mutations and their viral variants. *Cytokine Growth Factor Rev*. 2022:**63**:10–22.

Dwivedi R, Samanta P, Sharma P, Zhang F, Mishra SK, Kucheryavy P, Kim SB, Aderibigbe AOO, Linhardt RJ, Tandon R et al. Structural and kinetic analyses of holothurian sulfated glycans suggest potential treatment for SARS-CoV-2 infection. *J Biol Chem*. 2021:**297**(4):101207.

Farias WRL, Valente AP, Pereira MS, Mourão PAS. Structure and anticoagulant activity of sulfated galactans. Isolation of a unique sulfated galactan from the red algae *Botryocladia occidentalis* and comparison of its anticoagulant action with that of sulfated galactans from invertebrates. *J Biol Chem*. 2000:**275**(38):29299–29307.

Guimond SE, Mycroft-West CJ, Gandhi NS, Tree JA, Le TT, Spalluto CM, Humbert MV, Buttigieg KR, Coombes N, Elmore MJ et al. Synthetic heparan sulfate mimetic pixatimod (PG545) potently inhibits SARS-CoV-2 by disrupting the spike–ACE2 interaction. *ACS Cent Sci*. 2022:**8**(5):527–545.

Harvey WT, Carabelli AM, Jackson B, Gupta RK, Thomson EC, Harrison EM, Ludden C, Reeve R, Rambaut A, Peacock SJ et al. SARS-CoV-2 variants, spike mutations and immune escape. *Nat Rev Microbiol*. 2021:**19**(7):409–424.

Hu B, Guo H, Zhou P, Shi ZL. Characteristics of SARS-CoV-2 and COVID-19. *Nat Rev Microbiol*. 2020:**19**(3):141–154.

Kim SB, Zoepfl M, Samanta P, Zhang F, Xia K, Thara R, Linhardt RJ, Doerksen RJ, McVoy MA, Pomin VH. Fractionation of sulfated galactan from the red alga *Botryocladia occidentalis* separates its anticoagulant and anti-SARS-CoV-2 properties. *J Biol Chem*. 2022:**298**(5):101856.

Li JH, Li S, Zhi ZJ, Yan LF, Ye XQ, Ding T, Yan L, Linhardt RJ, Chen SG. Depolymerization of fucosylated chondroitin sulfate with a modified fenton-system and anticoagulant activity of the resulting fragments. *Mar Drugs*. 2016:**14**(9):170.

Li J, Li S, Yan L, Ding T, Linhardt RJ, Yu Y, Liu X, Liu D, Ye X, Chen S. Fucosylated chondroitin sulfate oligosaccharides exert anticoagulant activity by targeting at intrinsic tenase complex with low FXII activation: importance of sulfation 2 pattern and molecular size. *Eur J Med Chem*. 2017:**139**:191–200.

Mourão PAS. Perspective on the use of sulfated polysaccharides from marine organisms as a source of new antithrombotic drugs. *Mar Drugs*. 2015:**13**(5):2770–2784.

Oliveira SNMCG, Santos GRC, Glauser BF, Capillé NVM, Queiroz INL, Pereira MS, Pomin VH, Mourão PAS. Structural and functional analyses of biosimilar enoxaparins available in Brazil. *Thromb Haemost*. 2015:**113**(1):53–65.

Pereira MS, Mulloy B, Mourã PAS. Structure and anticoagulant activity of sulfated fucans. Comparison between the regular, repetitive, and linear fucans from echinoderms with the more heterogeneous and branched polymers from brown algae. *J Biol Chem*. 1999:**274**(12):7656–7667.

Planas D, Veyer D, Baidaliuk A, Staropoli I, Guivel-Benhassine F, Rajah MM, Planchais C, Porrot F, Robillard N, Puech J et al. Reduced sensitivity of SARS-CoV-2 variant Delta to antibody neutralization. *Nature*. 2021:**596**(7871):276–280.

Saito A, Irie T, Suzuki R, Maemura T, Nasser H, Uriu K, Kosugi Y, Shirakawa K, Sadamasu K, Kimura I et al. Enhanced fusogenicity and pathogenicity of SARS-CoV-2 Delta P681R mutation. *Nature*. 2021:**22**(11):1–7.

Shyr ZA, Gorshkov K, Chen CZ, Zheng W. Drug discovery strategies for SARS-CoV-2. *J Pharmacol Exp Ther*. 2020:**375**(1):127–138.

Tandon R, Sharp JS, Zhang F, Pomin VH, Ashpole NM, Mitra D, McCandless MG, Jin W, Liu H, Sharma P et al. Effective inhibition of SARS-CoV-2 entry by heparin and enoxaparin derivatives. *J Virol*. 2021:**95**(3):e01987–e01920.

Thakur S, Sasi S, Pillai SG, Nag A, Shukla D, Singhal R, Phalke S, Velu GSK. SARS-CoV-2 mutations and their impact on diagnostics, therapeutics and vaccines. *Front Med*. 2022:**9**:815389.

Tian D, Sun Y, Zhou J, Ye Q. The global epidemic of the SARS-CoV-2 Delta variant, key spike mutations and immune escape. *Front Immunol*. 2021:**12**:751778.

Vasconcelos AA, Sucupira ID, Guedes AL, Queiroz IN, Frattani FS, Fonseca RJ, Pomin VH. Anticoagulant and antithrombotic properties of three structurally correlated sea urchin sulfated glycans and their low-molecular-weight derivatives. *Mar Drugs*. 2018:**16**(9):304.

Wu M, Wen D, Gao N, Xiao C, Yang L, Xu L, Lian W, Peng W, Jiang J, Zhao J. Anticoagulant and antithrombotic evaluation of native fucosylated chondroitin sulfates and their derivatives as selective inhibitors of intrinsic factor Xase. *Eur J Med Chem*. 2015:**92**:257–269.

Xiu S, Dick A, Ju H, Mirzaie S, Abdi F, Cocklin S, Zhan P, Liu X. Inhibitors of SARS-CoV-2 entry: current and future opportunities. *J Med Chem*. 2020:**63**(21):12256–12274.

Yan L, Song Y, Xia K, He P, Zhang F, Chen S, Pouliot R, Weiss DJ, Tandon R, Bates JT et al. Heparan sulfates from bat and human lung and their binding to the spike protein of SARS-CoV-2 virus. *Carbohydr Polym*. 2021:**260**:117797.